Volcanic Climate Warming through Radiative and Dynamical Feedbacks of SO_2 Emissions

Scott D. Guzewich[1,6]*, Luke D. Oman[1,6], Jacob A. Richardson[2,1,5,6], Patrick L. Whelley[2,1,5,6], Sandra T. Bastelberger[2,1,5,6], Kelsey E. Young[1], Jacob E. Bleacher[3,1], Thomas J. Fauchez[4,1,6], Ravi K. Kopparapu[1,6]

[1]NASA Goddard Space Flight Center; Greenbelt, MD, USA.
[2]University of Maryland, College Park, MD, USA.
[3]NASA Headquarters, Washington, DC, USA.
[4]Universities Space Research Association, Columbia, MD, USA.
[5]Center for Research and Exploration in Space Science and Technology, NASA/GSFC, Greenbelt, MD, USA 20771
[6]NASA GSFC Sellers Exoplanet Environments Collaboration, Greenbelt, MD, USA 20771

Corresponding author: Scott D. Guzewich (scott.d.guzewich@nasa.gov)

Key Points:

- Volcanic emission of SO_2 produces warming through climate feedbacks.
- The warming is driven by a three orders of magnitude increase in stratospheric H_2O vapor.
- Climate cooling by H_2SO_4 aerosols persists for less time than the eruption itself.

Abstract

Volcanic flood basalt eruptions have been linked to or are contemporaneous with major climate disruptions, ocean anoxic events, and mass extinctions throughout at least the last 400M years of Earth's history. Previous studies and recent history have shown that volcanically-driven climate cooling can occur through reflection of sunlight by H_2SO_4 aerosols, while longer-term climate warming can occur via CO_2 emissions. We use the Goddard Earth Observing System Chemistry-Climate Model to simulate a four-year duration volcanic SO_2 emission of the scale of the Wapshilla Ridge member of the Columbia River Basalt eruption. Brief cooling from H_2SO_4 aerosols is outweighed by dynamically and radiatively driven warming of the climate through a three orders of magnitude increase in stratospheric H_2O vapor.

Plain Language Summary

Volcanic flood basalt eruptions are linked to mass extinctions and climate change through Earth's history. Using model experiments, we show that a massive release of sulfur dioxide gas, as would happen in such an eruption, can warm the climate through feedback mechanisms linked to an increase in stratospheric water vapor.

1 Introduction

Flood basalt eruptions are the largest in Earth's history by volume of emitted material (Rampino et al., 1998; Self et al., 2005; Reichow et al., 2009). They have covered vast areas with basalt, released massive amounts of climatically-relevant gases into the atmosphere, and are nearly contemporaneous with many of Earth's mass extinctions or ocean anoxic events (Wignall, 2001; Courtillot and Renne, 2003; Sobolev et al., 2011). Flood basalts appear common on other terrestrial worlds in the Solar System (Bond and Sun, 2021; Head et al., 2011; Lancaster et al., 1995; Jaeger et al., 2010; O'Hara, 2000). Unlike explosive eruptions of stratovolcanoes such as Toba, Tambora, and Pinatubo that last only for hours to weeks, flood basalt eruptions continue for years if not millenia (Courtillot and Renne, 2003; Jerram and Widdowson, 2005; Barry et al., 2010). The climate impact of such eruptions is still being debated in the literature with the cooling provided by shortwave sunlight reflection from H_2SO_4 aerosols balanced against the warming influence of CO_2 emissions (Self et al., 2005; Schmidt et al., 2016; Self et al., 2006; Black et al., 2018; Armstrong McKay et al., 2014). Such eruptions have been implicated in producing "hyperthermal" periods in Earth's history such as the Permian-Triassic hothouse and the Paleocene-Eocene Thermal Maximum, but the volume of emitted CO_2 seems insufficient for such warming (Bond and Sun, 2021; Gutjahr et al., 2017).

The Columbia River Basalt (CRB) eruption occurred 15-17 Ma in the Pacific Northwest of the United States (Kasbohm and Schoene, 2018; Reidel, 2015). It is the smallest continental flood basalt eruption and the most historically recent. It occurred near the Mid-Miocene Climatic Optimum (MMCO), a globally warm period with possibly enhanced atmospheric CO_2 levels, and just before the Mid-Miocene Climate Transition (MMCT), a period of cooling climate and increasing polar glaciation associated with a significant extinction event (Foster et al., 2012). The CRB has been proffered as a mechanism to drive either climate warming (as during the MMCO) or cooling (as during the MMCT) (Schmidt et al., 2016; Hodell and Wodruff, 1994; Kürschner et al., 2008; Sosdian et al., 2020). The Wapshilla Ridge member of the Grande Ronde basalt, one member of the CRB group, was responsible for 20% of the CRB's emitted volume and may have emitted up to 300 Gt of SO_2 into the atmosphere (Kasbohm and Schoene, 2018; Davis et al., 2017

). For reference, this amount is ~20,000 times the SO_2 emitted by the eruption of Mt. Pinatubo in 1991 (Bluth et al., 1992). CRB eruptions were likely a mix of explosive events that sent material high into the upper troposphere and lower stratosphere (~13-17 km altitude) and effusive eruptions that did not extend above 3 km altitude (Glaze et al., 2017).

Our study examines the climate response to the long duration and massive SO_2 release by such an eruption in the Goddard Earth Observing System Chemistry-Climate Model (GEOSCCM). A model such as GEOSCCM is needed to self-consistently model the conversion of SO_2 to H_2SO_4 aerosols, the radiative response to those aerosols, and the dynamical response to the eruption. Using the Wapshilla Ridge member of the CRB eruption as a template and scaling by 1/10, we emit 30 Gt of SO_2 into the model over four years through a 80%/20% mix of explosive and effusive eruptions, respectively (Davis et al., 2017, **Fig. S1**). We use a pre-industrial atmosphere with a fixed concentration of 280 ppm of CO_2, levels of ozone-depleting substances appropriate for the year 1850, and otherwise modern surface boundary and initial conditions to isolate the climate response to the SO_2 release through an eruption simulation and a baseline simulation without it. SO_2 is not radiatively active in the model.

2 Materials and Methods

We conduct two Goddard Earth Observing System Chemistry Climate Model (GEOSCCM) simulations for this work. The first is a baseline simulation without addition of volcanically-sourced SO_2. The second is the volcanic eruption scenario that releases SO_2 at model gridpoints in eastern Washington state and Oregon (corresponding to the CRB vents) following the volcanic eruption scenario detailed below. Both simulations run for 20 years. The simulations use modern initial and boundary conditions with a pre-industrial atmosphere. The atmosphere has a fixed CO_2 concentration of 280 ppm and ozone-depleting substances at levels appropriate for the year 1850. SO_2 is radiatively inert in the model.

2.1. Goddard Earth Observing System Chemistry Climate Model (GEOSCCM)

We use the GEOSCCM, which couples a general circulation model (Rienecker et al., 2008; Nielsen et al., 2017) with dynamic ocean and sea ice modules (Aquila et al., 2021) and a comprehensive Global Modeling Initiative (GMI) stratosphere-troposphere chemical mechanism (Duncan et al., 2007; Strahan et al., 2007), to assess the atmosphere-ocean-chemistry coupled response to a CRB-type volcanic perturbation. The model is integrated with the GOddard Chemistry, Aerosol, Radiation, and Transport (GOCART) bulk aerosol module (Colarco et al., 2010), to simulate aerosol evolution and transport and its effect on radiation.

The GMI chemical mechanism includes 117 species, 322 chemical reactions, and 81 photolysis reactions. The SMVGEAR II algorithm (Jacobson et al., 1995) is used to integrate the chemical mass balance equations. The mechanism includes a detailed description of O_3-NO_x-hydrocarbon chemistry, which is described in *(*Duncan et al., 2007*)*. In order to better understand the feedbacks to climate these simulations used a dynamic ocean, from the Modular Ocean Model, Version 5 (MOM5) (Griffies et al., 2005; Griffies et al., 2012), and the Los Alamos Sea Ice Model (CICE) (Hunke et al., 2008). The simulations used a horizontal resolution of 1° longitude by 1° latitude in the atmosphere and ocean components. The atmosphere has 72 vertical levels from the surface to ~80 km and the ocean component has 50 layers down to a depth of 4,500 m.

2.2. Columbia River Volcanic Eruption Scenario

Our Columbia River Flood Basalt eruption scenario is informed by the eruption dynamics of the Wapshilla Ridge Member of the Grande Ronde Basalt Group within the CRB. As the Wapshilla Ridge Member represents the largest flow unit of the Grande Ronde, which in turn was the largest phase of the CRB, this simulated eruption provides a high-end view of the short-term climate effects produced by the CRB. Total erupted SO_2 of the Wapshilla Ridge was likely 300 Gt (Kasbohm and Schoene, 2018; Davis et al., 2017) and thermal modeling informed by geothermal alteration of host rocks near Wapshilla vents provides an eruption duration of as low as 4 years (Davis et al., 2017). Assuming that the Wapshilla Ridge was formed through multiple eruptive episodes (e.g., Davis et al., 2017), our scenario erupts one-tenth of the total estimated SO_2 mass, 30 Gt, over 4 calendar years. Around 20% of the SO_2 delivered to that atmosphere during this eruptive phase passively outgassed from the lava flow itself, with the remaining 80% directly vented from the fissure. Following (Glaze et al., 2017), we assume that the Wapshilla fissure vents periodically erupted SO_2 into the Upper Troposphere-Lower Stratosphere (UTLS) from 13-18 km altitude. We deliver the final 20% of the gas to the Planetary Boundary Layer (PBL) and lower troposphere (<3 km altitude). To minimize seasonal effects, UTLS injections of SO_2 are divided into 4 discrete "eruptions" per year, equally spaced over each calendar. PBL injections, however, are constant.

3 Results

The initial response to the eruption is rapid cooling, particularly focused over northern hemisphere continental areas (**Fig. 1**). Global mean temperatures cool by 2-3 K in the first two years following the eruption. However, July and August monthly mean temperatures over northern hemisphere continents are 10-30 K colder than a baseline simulation (**Fig. S2**). The coldest temperature anomalies are in central and southwest Asia. Southern hemisphere continents experience more modest cooling in the first two years, but still experience temperatures 5-15 K below a baseline simulation, with the coldest area relative to normal in central South America south of the Amazon basin. Most of Antarctica's surface area warms 2-8 K, however. By the first northern hemisphere winter following the beginning of the eruption, these cold temperature anomalies are reversed and 8-15 K warm anomalies blanket the Arctic, Siberia, and north-central North America. Some 5-15 K cold anomalies remain over Australia, South Africa, and Argentina, but they are small in area relative to northern hemisphere summer. This winter warming and summer cooling is a well-known response to other volcanic eruptions, including Pinatubo (Kirchner et al., 1999). The summer cooling is a direct response to the reduction in incoming solar radiation by the volcanic aerosols, while the winter warming is a dynamically indirect response to a strengthened winter stratospheric polar vortex (Kirchner et al., 1999). This is true in our simulation as well with an extremely cold stratospheric winter polar vortex throughout the eruption years and for several years after. In fact, the stratospheric winter polar vortex sees temperatures as low as -158 to -168°C, cold enough to condense CO_2 (although such physics are not included in GEOSCCM).

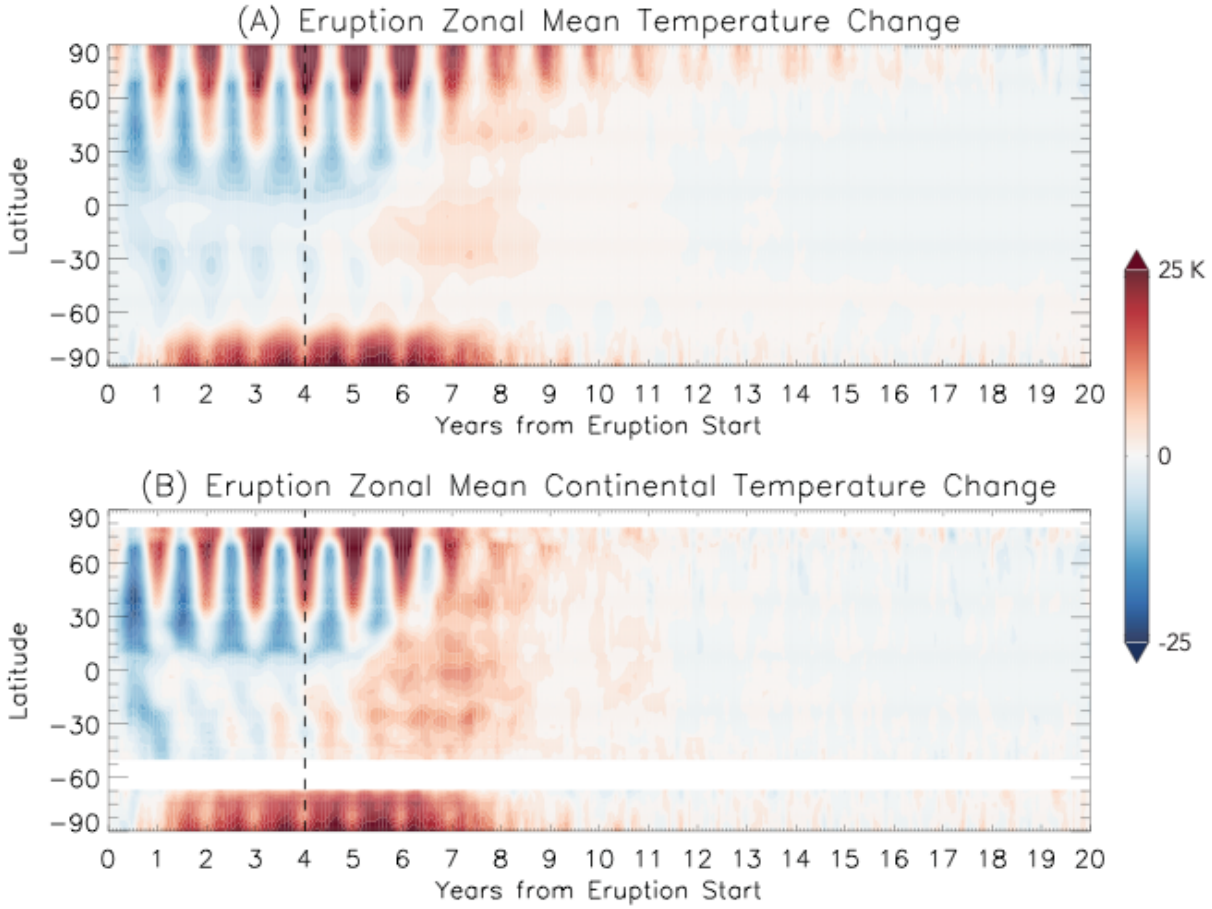

Fig. 1. Zonal mean temperature change of the eruption simulation relative to a baseline. (A) Zonal mean temperature change (K) of the eruption simulation relative to a 20-year average of a baseline simulation as a function of time and (B) the zonal mean temperature change over continental areas only. The vertical dashed line represents the end of the eruption.

The cooling response to large volcanic eruptions is well-known in the literature and in modern history (Schmidt et al., 2016; Self et al., 2006; Black et al., 2018; Kirchner et al., 1999; Stoffel et al., 2015; Robock, 2000). SO_2 is rapidly and efficiently converted to H_2SO_4 aerosols, which are optically reflective and scatter incoming solar shortwave radiation back to space (Robock, 2000). Indeed, the volume of emitted SO_2 is so large that the global area-weighted H_2SO_4 550 nm aerosol optical thickness (AOT) exceeds 40 at the end of the first year following the start of the eruption. At the conclusion of the eruption in year four, global mean AOT reaches almost 220 (**Fig. S3**). The thickest aerosol layer remains concentrated in the northern hemisphere throughout the eruption and extends throughout the troposphere and stratosphere. Even the northern hemisphere surface atmosphere has part-per-million (ppm) level H_2SO_4 aerosol mixing ratios with the maximum aerosol concentrations occurring at 200 hPa.

This extremely opaque aerosol layer radically alters the planet's net radiative budget (**Fig. S4, S5**). It drives a 140-150 W/m^2 reduction in surface downward shortwave radiation flux and a somewhat larger (180 W/m^2) decrease in planetary outgoing longwave radiation. Concurrently, there is a

brief 35% reduction in global cloud cover (**Fig. S5**) with a nearly order-of-magnitude reduction in precipitation rate (**Fig. S6**). Past research has also implied that large volcanic eruptions reduce monsoon intensity in the northern hemisphere (Zambri et al., 2017). Our eruption simulation similarly sees a drastic reduction of Indian and southeast Asian monsoon precipitation (and throughout the northern hemisphere summer intertropical convergence zone) during the eruption and for 4-6 years after, before a multiyear period with enhanced monsoon precipitation coinciding with the warmest global temperature anomalies (**Fig. S7**). We also see dramatically increased precipitation in South America, particularly the Pacific coast of Ecuador and Peru.

Despite the initial near-surface cooling, the very thick H_2SO_4 aerosol layer efficiently absorbs longwave radiation from the surface (Kirchner et al., 1999) and warms the troposphere and stratosphere. Tropical (20°S-20°N) temperature profiles warm through the troposphere and become more stable. However, this warming also completely eliminates the tropical tropopause—the atmosphere's cold trap for water vapor. Tropical tropopause temperatures warm by as much as 60 K and this occurs rapidly following the initial months of the eruption, even while the surface and lower troposphere are still cooling (**Fig. 2**). Indeed, during and continuing for almost four years after the end of the eruption, there is no tropical temperature inversion in monthly mean vertical temperature profiles. Despite a less convectively unstable vertical temperature profile, the complete lack of a temperature inversion allows water vapor to flood into the stratosphere. Starting almost immediately after the eruption begins, stratospheric water vapor levels increase by up to three orders-of-magnitude (**Fig. 3**), reaching part-per-thousand mixing ratios, neatly following the Clausius-Clapeyron relation for such a temperature change in the upper troposphere and stratosphere.

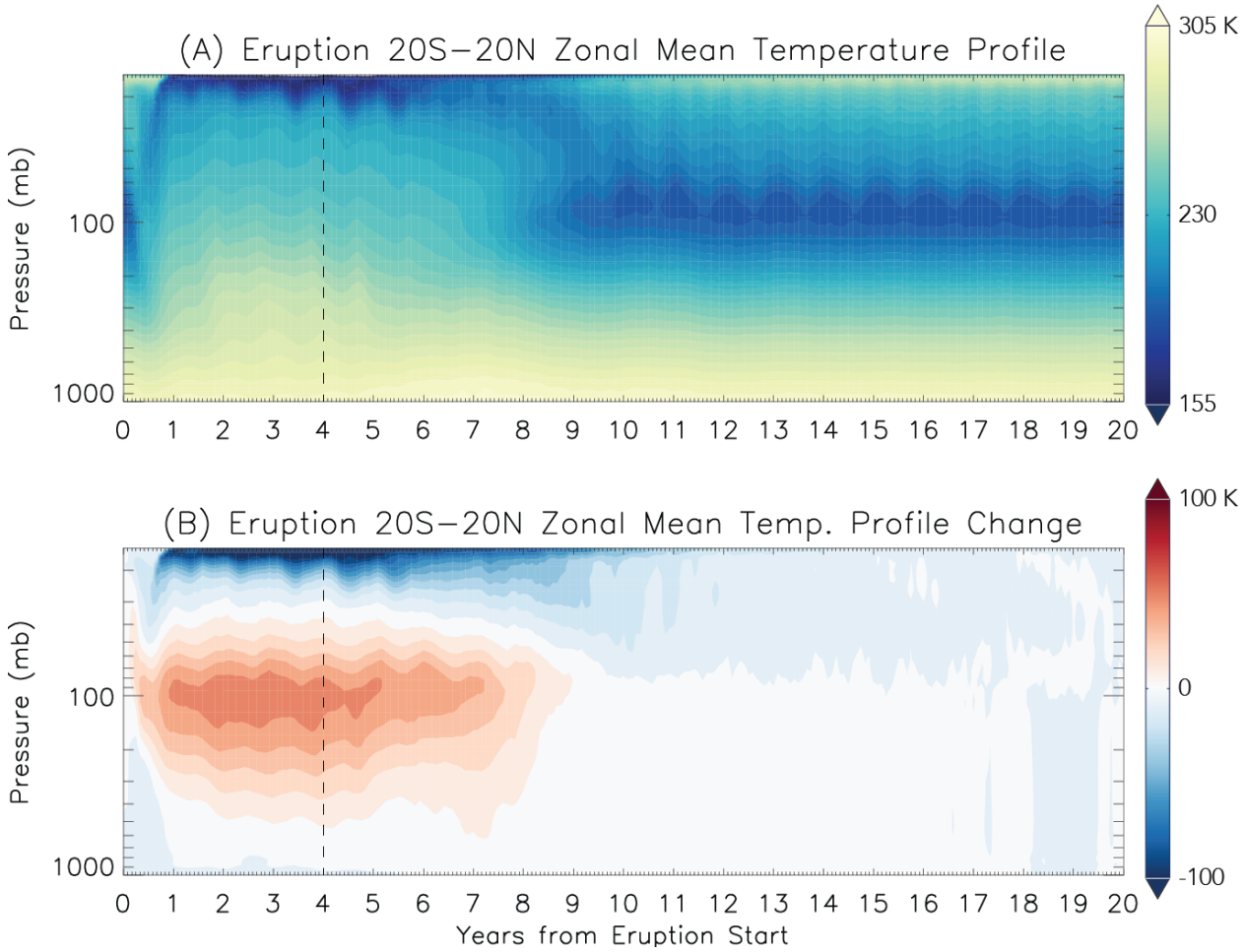

Fig. 2. Vertical temperature profile response to the eruption. (A) Zonal mean vertical temperature (K) profile in the tropics (20°S-20°N) of the eruption simulation as a function of time and pressure and (B) the change in the vertical temperature profile relative to a baseline simulation. The vertical dashed line represents the end of the eruption.

It is this change to stratospheric water vapor mixing ratios that is responsible for the subsequent climate warming. Rather than having a strengthening net cooling response due to the increasing aerosol optical thickness over the four years of the eruption, downward longwave flux from this stratospheric water vapor counteracts the reduction in surface shortwave flux. This water vapor provides 50 W/m^2 of downward longwave flux at the surface when the stratospheric water vapor mixing ratio is maximized. This causes global mean surface temperatures to return to those of the baseline simulation prior to the end of the eruption, late in the fourth year of the simulation. Global temperatures continue to warm well past the end of the eruption, peaking nearly four years later with global mean surface temperature anomalies of +5-6 K (**Fig. 1**). At this point, typical seasonality also returns to global mean temperatures with an annual minimum in northern hemisphere winter and maximum in northern summer.

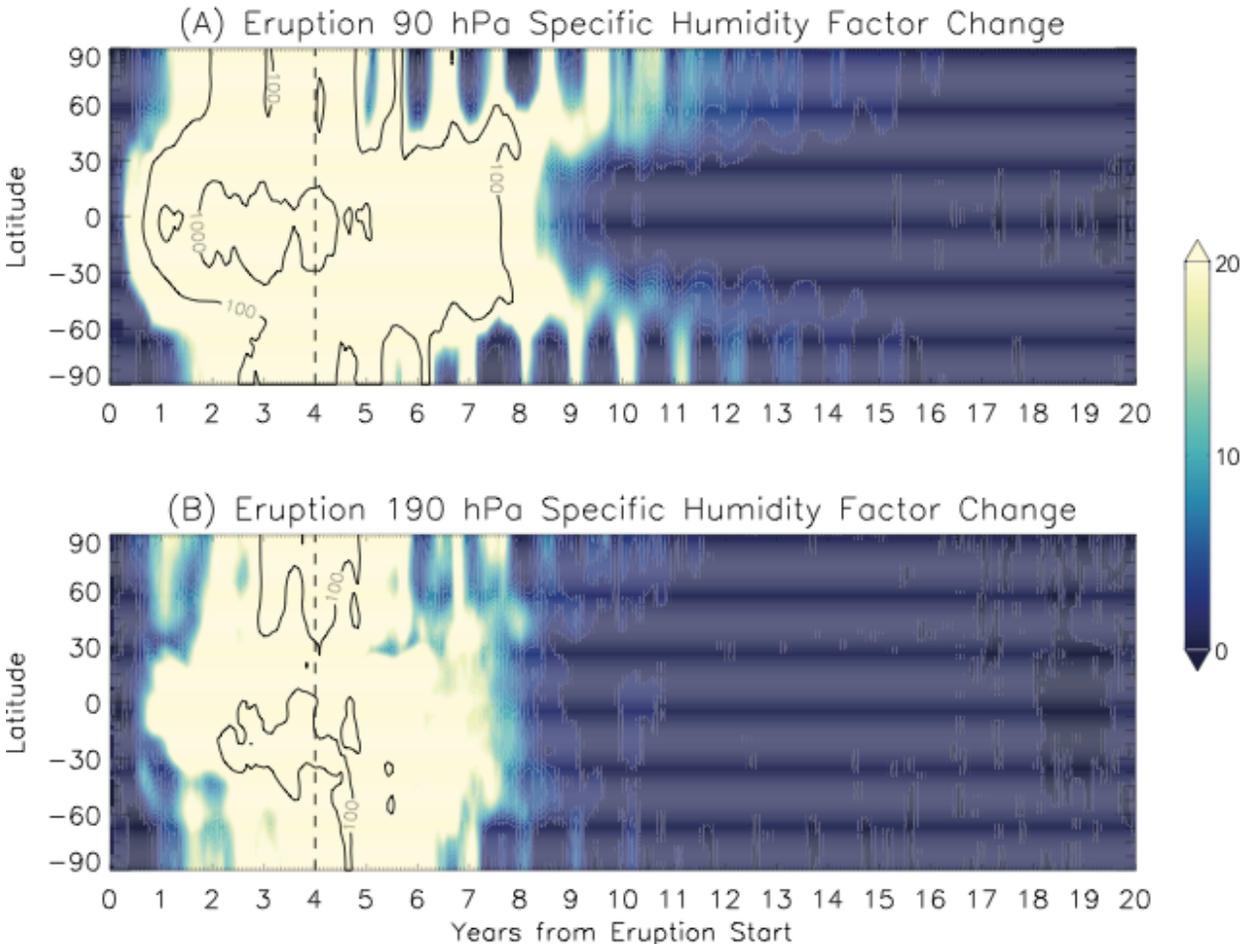

Fig. 3. Stratospheric water vapor increases as a result of the eruption. (A) Factor change in the zonal mean specific humidity at the 90 hPa pressure level in the eruption simulation relative to the baseline simulation as a function of time and (B) the same at the 190 hPa pressure level. Locations with 100 and 1000 times the specific humidity of the baseline simulation are indicated within the solid black contours. The vertical dashed line represents the end of the eruption.

As was the case with the initial global cooling following the eruption, the subsequent climate warming is regionally variable. The combination of the downwelling longwave from the increased stratospheric water vapor and the very cold and consolidated stratospheric winter polar vortex drives 15-30 K warm anomalies in January in northern North America and Siberia four years after the eruption ends (**Fig. 1, Fig. S8**). In July of simulation year 8, +10-20 K anomalies occurred on all continents with widespread +20-25 K in Antarctica. Nearly all continental areas on the planet have warmer than normal temperatures for years 5-13 of the simulation (1-9 years after the eruption ends). Continental areas with extreme heat (monthly mean temperatures ≥40°C) are dramatically expanded. In January of simulation year 8, such areas occur throughout the Amazon basin, south central South America, central and southern Africa, and much of central Australia. Monthly mean temperatures in some areas (the Amazon and east-central Australia) reach 49°C. July mean temperatures equal or exceed 40°C for the Sahara, the Arabian peninsula, and northwest portions of the Indian subcontinent, with extreme monthly mean temperatures ≥55°C in southwest

Asia (**Fig. S8**). Even central North America has a small area with monthly mean temperatures of 40°C in July of simulation year 8.

Faster atmospheric circulation (limiting formation), removal of the tropical tropopause, and subsequent moistening and cooling of the stratosphere produces massive ozone destruction. Our simulations were conducted with a pre-industrial atmosphere, hence there is no anthropogenic chlorine to catalyze ozone destruction. Global ozone loss averages 185 Dobson units (DU) during simulation years 3-11, with middle and high latitude ozone loss exceeding 300 DU during winter (**Fig. S9**).

Ocean circulation changes as well, with a general global slowing of near-surface current patterns. The major currents of the northern hemisphere such as the Gulf Stream and Kuroshio are slowed by 0.2-0.4 m/s, while the entire North Pacific gyre is displaced southward which weakens the north equatorial current. The Antarctic Circumpolar current and the East Australian Current are least impacted, but also see modest (~0.1 m/s) slowing. Reduced precipitation over continental areas leads to reduced freshwater river discharge and salinification of the Arctic, North Atlantic, and North and West-Equatorial Pacific oceans.

Despite these volatile changes to planetary climate during and following the eruption, conditions return to or near pre-eruption by 11-16 years after the eruption ends. The H_2SO_4 aerosol is removed even faster, and is completely gone from the atmosphere four years after the end of the eruption (**Fig. S2**). Global surface temperatures return to within a few degrees of the baseline simulation (**Fig. 1**), stratospheric water vapor mixing ratios return to ~3 ppm (**Fig. 3**), and the ozone layer recovers (**Fig. S9**).

4 Discussion and Conclusion

With SO_2 emissions alone, our results support the CRB eruption as an agent that helped drive the warm temperatures of the MMCO. Existing climate studies of the middle Miocene have had trouble reconciling geological proxy evidence of warm global temperatures (~3°C above present) with those of high, but not excessive CO_2 abundances (~350-400 ppm) (Tong et al., 2009; You et al., 2009; Goldner et al., 2014; Henrot et al., 2010; Burls et al., 2021). Those studies have often suggested changes in continental topography and albedo as well as ocean circulation differences (associated with the open Central American and East Tethys Seaways (Henrot et al., 2010; Herold et al., 2011)) as additional agents of climate warming. The literature suggests that up to 2°C of warming is possible through the use of Miocene-appropriate surface and boundary conditions alone (Burls et al., 2021). Our study did not aim to directly reproduce Miocene climate as we used modern pre-industrial boundary conditions. Still, the warmth produced by SO_2 emissions from the CRB eruptions, concentrated most strongly in the northern hemisphere continents and oceans, could help to reconcile insufficiently low global CO_2 levels with regionally-variable climate responses. Periodic eruptions of the CRB, which may have been phased over thousands or even millions of years (Kasbohm and Schoene, 2018), would have helped generate this intermittent warming response driven by stratospheric water vapor increases. Presumably (although further simulations are needed to confirm), the addition of CO_2 emissions would only enhance this warming and possibly help mitigate the initial cooling response seen in our eruption simulation.

Indeed, thermal maxima or hyperthermal events have occurred concurrently or near in time to several flood basalt eruptions/large igneous province emplacements through Earth's history. These include the Permian-Triassic, Paleocene-Eocene, and others and have been linked to major

eruptions such as the Siberian Traps and North Atlantic Igneous Province, respectively (Bond and Sun, 2021; Gutjahr, 2017). As with the MMCO and CRB, a great deal of CO_2 is necessary to match paleotemperature proxies from these events, and there remains a dispute if sufficient CO_2 was emitted to explain these warm climates (Sobolev et al., 2011; Self et al., 2006; Armstrong McKay et al., 2014). Black et al. (2018) modeled the Siberian Trap eruption climate impact and found swings in climate between cooler sulfur-dominated periods and longer warm carbon-dominated periods, however they did not include sulfur aerosol radiative heating which precluded the tropopause warming that let water vapor flood into the stratosphere in our simulation. While our results are consistent with sulfur emissions producing short-duration climate responses, we show that sulfur alone can initiate climate warming, that is more intense and longer-lasting than the brief cooling from shielding of shortwave radiation by sulfate aerosols, through the dynamical and radiative response to stratospheric water vapor increases.

Our simulations thus challenge previous work that showed substantial decade-long climate cooling from sulfur emissions (and hence sulfate aerosols) alone (Schmidt et al., 2016; Self et al. 2006). The brief cooling we do see in the simulation within the first 1-3 years also does not increase land or sea ice cover in a way that suggests sulfate aerosol cooling could initiate a positive feedback with glaciation. North polar sea ice is above normal in area and does not exhibit seasonal melting during the first 4 years of the simulation, but drops below normal for several years after the eruption before then recovering. Similarly, widespread continental snow cover persists year-round for much of northern Canada and Siberia during the eruption and immediately after, which would tend to support glacial growth. However, the subsequent climate warming melts that snow cover within ~3 years after the end of the eruption and eliminates that nascent development before it could possibly reinforce the cooling through feedback processes.

These rapid climate variations would present challenges to the biosphere. The very high continental summer temperatures would stress mammals with areas of >31°C wet bulb globe temperatures expanded accordingly beyond baseline conditions. The likely fatal threshold of 35°C wet bulb globe temperature for mammals is not exceeded anywhere on a monthly mean basis, although transient periods with that level are possible (Sherwood et al., 2010). The increase and then subsequent decrease in sea ice, coupled with a lack of seasonality could disrupt those ecosystems dependent on sea ice. The ozone destruction would tend to increase surface ultraviolet flux, but the presence of the H_2SO_4 aerosol layer, at least partially, ameliorates that threat. The Siberian Traps eruption may have produced massive ozone destruction, primarily through the concurrent emission of chlorinated species, which led to mutations among palynomorphs (Beerling et al., 2007).

Mass extinctions and ocean anoxic events are closely correlated with flood basalt eruption/large igneous province emplacement through the last 400 Ma of Earth's history. During the Miocene, a comparatively modest extinction event occurred, often termed the "Middle Miocene disruption" (Rapu et al., 1986). It followed the MMCO and was concurrent with the cooling of the MMCT. Given our results, it seems more plausible that other factors following the CRB eruption (e.g., the drawdown of CO_2 and the end of transient additional warming through the response to SO_2 emissions) were proximate to the extinction, rather than cooling driven by volcanic aerosols from the CRB eruptions. However, most of the past extinctions associated with flood basalt eruptions are believed to be due to associated climate warming (Reichow et al., 2009; Wignall, 2001; Courtillot and Renne, 2003; Sobolev et al., 2011; Bond and Sun, 2021). Indeed, past mass

298 extinctions are correlated with ≥5.2°C temperature increases, which our eruption simulation briefly
299 exceeds (Song et al., 2021).

300 The amount of water vapor in the stratosphere is a key metric for evaluating the evolution of any
301 terrestrial planet. Kasting et al. (1993) found a moist greenhouse limit of 3 parts-per-thousand
302 volume mixing ratio of H_2O vapor in the stratosphere based on diffusion-limited calculations of H
303 loss to space. Various three-dimensional climate models have found similar results with warm
304 (>320 K) surface temperatures (Wolf and Toon, 2015; Way et al., 2018; Popp et al., 2015) for a
305 rapidly-rotating planet like Earth, although that result is not uniform across all models (Leconte et
306 al., 2013). As the stratospheric water vapor mixing ratio in our eruption simulation exceeds this
307 threshold, our results point toward volcanically-induced transient moist greenhouse conditions
308 during major flood basalt eruptions. While planetary water loss through high altitude
309 photodissociation and escape may never have been a problem for Earth, that process is ongoing
310 for Mars and Venus. The role of volcanism in the evolution of climate and planetary water
311 inventory for both worlds is much debated (e.g., Solomon et al., 1999; Halevy and Head, 2014;
312 Kerber et al., 2015) and the possibility of exceeding the moist greenhouse limit during and
313 following major eruptions suggests possibly counteracting results. While a major eruption could
314 lead to periods of climate warmth for, e.g., early Mars, it may have also accelerated planetary water
315 loss by increasing the amount of water vapor at high altitudes that is more susceptible to
316 photodissociation and escape of hydrogen. Interestingly, (Bardeen et al., 2017) found similar
317 stratospheric moistening and ozone destruction while simulating the climate impacts of a major
318 asteroid impact and ejection of ~15 Tg of soot into the atmosphere due to the subsequent global
319 fires, as well as a comparable ~15 year duration to return to pre-event climate conditions.

320 Increases in stratospheric water vapor following volcanic eruptions has been measured after
321 Pinatubo and modeled for larger eruptions (Robock et al., 2009; Löffler et al., 2016; Joshi et al.,
322 2003). But the short duration of such eruptions prevents the removal of the tropical tropopause as
323 was seen in our simulation, and avoids a greater moistening of the stratosphere. Our results imply
324 that the long duration of flood basalt eruptions drives unique climate responses that do not occur
325 from classic stratovolcano eruptions such as Pinatubo, Toba, and Tambora. The long duration and
326 massive quantity of SO_2 emitted over years drives circulation responses that are ultimately more
327 impactful to the climate than the simple radiative response to the H_2SO_4 aerosols. Ultimately, the
328 difference in e-folding time in the removal of H_2SO_4 aerosols and that of the stratospheric water
329 vapor is a key metric. The sulfate aerosols are removed faster than water vapor from the
330 stratosphere, which allows the warming effect of the water vapor to dominate and persist longer
331 than the cooling provided by sulfate aerosol. Cooling from sulfate aerosols in our simulation
332 persists no longer than the eruption itself due to this fundamental difference in removal timescales.
333 This suggests that the "volcanic winter" (analogous to "impact winters" (Vellekoop et al., 2014))
334 paradigm of long-duration cold and darkness in response to massive flood basalt eruptions should
335 be reconsidered, and that any cooling is brief (although perhaps regionally intense) before a more
336 significant and long-duration warm response.

337 **Acknowledgments**

338 GEOSCCM is supported by the NASA MAP program and the high-performance computing
339 resources were provided by the NASA Center for Climate Simulation (NCCS).
340

Open Research

GEOSCCM model output is available on Zenodo at doi: 10.5281/zenodo.5420632.

References

Aquila, A., C. Baldwin, N. Mukherjee, E. Hackert, F. Li, J. Marshak, et al., Impacts of the eruption of Mount Pinatubo on surface temperatures and precipitation forecasts with the NASA GEOS subseasonal-to-seasonal system, *Journal of Geophysical Research: Atmospheres* **126**, e2021JD034830 (2021). doi: 10.1029/2021JD034830

Armstrong McKay, D.I., T. Tyrrell, P.A. Wilson, G.L. Foster, Estimating the impact of the cryptic degassing of Large Igneous Provinces: A mid-Miocene case-study, *Earth Planet. Sci. Lett*. **403**, 254–262 (2014).

Bardeen, C.G., R.R. Garcia, O.B. Toon, A.J. Conley, On Transient Climate Change at the Cretaceous-Paleogene Boundary due to Atmospheric Soot Injections, *Proceedings of the National Academy of Sciences of the United States of America* **114**, 36, E7415-7424 (2017). doi:10.1073/pnas.1708980114

Barry, T.L., S. Self, S.P. Kelley, S. Reidel, P. Hooper, and M. Widdowson, New $^{40}Ar/^{39}Ar$ dating of the Grande Ronde lavas, Columbia River Basalts, USA: Implications for duration of flood basalt eruption episodes, Lithos **118**, 3-4, 213-222 (2010). https://doi.org/10.1016/j.lithos.2010.03.014.

Beerling, D.J., M. Harfoot, B. Lomax, J.A. Pyle, The stability of the stratospheric ozone layer during the end-Permian eruption of the Siberian Traps, *Phil. Trans. R. Soc. A.* **365,** 1843–1866 (2007), http://doi.org/10.1098/rsta.2007.2046

Black, B.A., R.R. Neely, JF Lamarque, *et al.,* Systemic swings in end-Permian climate from Siberian Traps carbon and sulfur outgassing, *Nature Geosci* **11**, 949–954 (2018). https://doi.org/10.1038/s41561-018-0261-y

Bluth, G.J.S., S.D. Doiron, C.C. Schnetzler, A.J. Krueger, L.S. Walter, Global Tracking of the SO_2 Clouds from the June, 1991 Mount Pinatubo Eruptions, *Geophysical Research Letters* **19**(2), 151-154 (1992). doi: 10.1029/91GL02792.

Burls, N.J., C.D. Bradshaw, A.M. De Boer, N. Herold, M. Huber et al., Simulating Miocene warmth: Insights from an opportunistic multi-model ensemble (MioMIP1). *Paleoceanography and Paleoclimatology* **36**, e2020PA004054 (2021). https://doi.org/10.1029/2020PA004054

Colarco, P., A. Da Silva, M. Chin, T. Diehl, Online simulations of global aerosol distributions in the NASA GEOS-4 model and comparisons to satellite and ground-based aerosol optical depth, *J. Geophys. Res*. **115**(D14), D14207 (2010). doi:10.1029/2009JD012820.

Courtillot, V.E., P. R. Renne, On the ages of flood basalt events, *C. R. Geosci.* **335**, 113–140 (2003).

Davis, K.N., J. A. Wolff, M. C. Rowe, O. K. Neill, Sulfur release from main-phase Columbia River Basalt eruptions, *Geology* **45** (11), 1043–1046 (2017). doi: https://doi.org/10.1130/G39371.1

Duncan, B.N., S.E. Strahan, Y. Yoshida, S.D. Steenrod, N. Livesey, Model study of cross-tropopause transport of biomass burning pollution, *Atmos. Chem.* Phys., 7, 3713-3736 (2007).

Foster, G.L., C.H. Lear, J.W.B. Rae, The evolution of pCO2, ice volume and climate during the middle Miocene, *Earth Planet. Sci. Lett* **341–344**, 243–254 (2012).

Glaze, L.S.,S. Self, A. Schmidt, S.J. Hunter, Assessing Eruption Column Height in Ancient Flood Basalt Eruptions, *Earth and Planetary Science Letters* **457**, 263-270 (2017). doi: 10.1016/j.epsl.2014.07.043.

Goldner, A., N. Herold, M. Huber, The Challenge of Simulating the Warmth of the mid-Miocene Climatic Optimum in CESM1, *Climate of the Past* **10**, 523-536 (2014). doi: 10.5194/cp-10-523-2014

Griffies, S.M., A. Gnanadesikan, K.W. Dixon, J.P. Dunne, R. Gerdes, M.J. Harrison, et al., Formulation of an ocean model for global climate simulations, *Ocean Science* **1**, 45-79 (2005).

Griffies, S.M., R. J. Greatbatch, Physical processes that impact the evolution of global mean sea level in ocean climate models, *Ocean Modelling* **51**, 37-72 (2012). doi:10.1016/j.ocemod.2012.04.003.

Gutjahr, M., A. Ridgwell, P. Sexton, *et al.,* Very large release of mostly volcanic carbon during the Palaeocene–Eocene Thermal Maximum, *Nature* **548**, 573–577 (2017). https://doi.org/10.1038/nature23646

Halevy, I., J. Head III, Episodic warming of early Mars by punctuated volcanism. *Nature Geosci* **7**, 865–868 (2014). doi:10.1038/ngeo2293

Head III, J.W., et al., Flood Volcanism in the Northern High Latitudes of Mercury Revealed by MESSENGER, *Science* **333** (6051), 1853-1856 (2011). doi: 10.1126/science.1211997.

Henrot, A.-J., L. François, E. Favre, M. Butzin, M. Ouberdous, G. Munhoven, Effects of CO_2, continental distribution, topography and vegetation changes on the climate at the Middle Miocene: a model study, *Clim. Past* **6**, 675–694 (2010). https://doi.org/10.5194/cp-6-675-2010

Herold, N., M. Huber, R.D. Müller, Modeling the Miocene Climatic Optimum. Part I: Land and Atmosphere, *Journal of Climate* **24**(24), 6353-6372 (2011). doi: 10.1175/2011JCLI4035.1

Hodell, D.A., F. Wodruff, Variations in the strontium isotopic ratio of seawater during the Miocene: stratigraphic and geochemical implications, *Paleoceanography* **9**, 405-426 (1994).

Hunke, E.C., W. H. Lipscomb, "CICE: The Los Alamos Sea Ice Model, Documentation and Software Manual, Version 4.0" (Technical Report, Los Alamos National Laboratory, 2008).

Jacobson, M.Z., Computation of global photochemistry with SMVGEAR II, *Atmos. Environ*. **29**, 2541–2546 (1995).

Jaeger, W.L. et al., Emplacement of the youngest flood lava on Mars: A short, turbulent story, *Icarus* **205**(1), 230-243 (2010). https://doi.org/10.1016/j.icarus.2009.09.011.

Jerram, D.A., M. Widdowson, The anatomy of Continental Flood Basalt Provinces: geological constraints on the processes and products of flood volcanism, Lithos **79**, 3-4 385-405 (2005). https://doi.org/10.1016/j.lithos.2004.09.009.

Joshi, M.M., K.P. Shine, A GCM Study of Volcanic Eruptions as a Cause of Increased Stratospheric Water Vapor, *Journal of Climate* **16**(21), 3525-3534 (2003). doi: 10.1175/1520-0442(2003)016<3525:AGSOVE>2.0.CO;2

Kasbohm, J., B. Schoene, Rapid eruption of the Columbia River flood basalt and correlation with the mid-Miocene climate optimum, *Science Advances* **4**(9), eaat8223 (2018). doi: 10.1126/sciadv.aat8223

Kasting, J.F., D.P. Whitmire, R.T. Reynolds, Habitable Zones Around Main Sequence Stars, *Icarus* **101**, 1, 108-128 (1993). doi: 10.1006/icar.1993.1010

Kerber, L., F. Forget, R. Wordsworth, Sulfur in the Early Martian Atmosphere Revisted: Experiments with a 3-D Global Climate Model, *Icarus* **261**, 133-148 (2015). doi:10.1016/j.icarus.2015.08.011

Kirchner, I., G.L. Stenchikov, H.-F. Graf, A. Robock, A., J.C. Antuña, Climate model simulation of winter warming and summer cooling following the 1991 Mount Pinatubo volcanic eruption, *J. Geophys. Res.* **104**(D16), 19039–19055 (1999). doi:10.1029/1999JD900213.

Kürschner, W.M., Z. Kvacek, D.L. Dilcher, The impact of Miocene atmospheric carbon dioxide fluctuations on climate and the evolution of terrestrial ecosystems, *Proc. Natl. Acad. Sci*. **105**, 440-453 (2008).

Lancaster, M.G., et al., Great Lava Flow Fields on Venus, *Icarus* **118**(1), 69-86 (1995). https://doi.org/10.1006/icar.1995.1178.

Leconte, J., F. Forget, B. Charnay *et al.*, Increased insolation threshold for runaway greenhouse processes on Earth-like planets, *Nature* **504**, 268–271 (2013). doi: 10.1038/nature12827

Löffler, M., S. Brinkop, P. Jöckel, Impact of major volcanic eruptions on stratospheric water vapour, *Atmos. Chem. Phys.* **16**, 6547–6562 (2016). doi:10.5194/acp-16-6547-2016

Nielsen, J.E., S. Pawson, A. Molod, B. Auer, A. M da Silva, A. R. Douglass, B. Duncan, Q. Liang, M. Manyin, L. D. Oman, W. Putman, S. E. Strahan, K. Wargan, Chemical mechanisms and their applications in the Goddard Earth Observing System (GEOS) earth system model, *J. Adv. Model. Earth Syst.* **9**, 3019–3044 (2017). doi:10.1002/2017MS001011

O'Hara, M.J., Flood Basalts and Lunar Petrogenesis, *Journal of Petrology* **41**(7), 1121-1125 (2000)..

Popp, M.,H. Schmidt, J. Marotzke, Transition to a Moist Greenhouse with CO2 and solar forcing, *Nat Commun* **7**, 10627 (2016). doi:10.1038/ncomms10627

Rampino, M.R., R.B. Stothers, Flood Basalt Volcanism During the Past 250 Million Years, *Science* **241**, 4866, 663-668 (1998). doi:10.1126/science.241.4866.663.

Raup, D.M., J.J. Sepkoski Jr., Periodic Extinction of Families and Genera, *Science* **231**, 4740, 833-836 (1986). doi: 10.1126/science.11542060.

Reichow, M.K., A.D. Saunders, M.S. Pringle, A.I. Al'Mukhamedov, A.Y.Medvedev, M.B. Allen, V.L. Andreichev, M.M. Buslov, G.S. Fedoseev, I.Y. Safonova, C.E.Davies, J.G. Fitton, S. Inger, C. Mitchell, V.N. Puchkov, R.A. Scott, The timing and extent of the eruption of the Siberian Traps large igneous province: Implications for the end-Permian environmental crisis, *Earth Planet. Sci. Lett.* **277** (1–2), 9-20 (2009).

Reidel, S.P., The Columbia River Basalt Group: A flood basalt province in the Pacific Northwest, USA, *Geosci. Can.* **42**, 151–168 (2015).

Rienecker, M.M., et al., "The GEOS-5 data assimilation system — Documentation of versions 5.0.1, 5.1.0, and 5.2.0" (NASA Tech. Memo., NASA TM-2008-104606, vol. 27, 118 pp, 2008)

Robock, A., Volcanic eruptions and climate, *Reviews of Geophysics* **38**, 191–219 (2000).

Robock, A., C.M. Ammann, L. Oman, D. Shindell, S. Levis, and G. Stenchikov, Did the Toba volcanic eruption of ~74k BP produce widespread glaciation? *J. Geophys. Res.* **114**, D10107 (2009). doi:10.1029/2008JD011652.

Schmidt, A., R.A. Skeffington, T. Thordarson, S. Self, P.M. Forster, A. Rap, et al., Selective environmental stress from sulphur emitted by continental flood basalt eruptions, *Nature Geoscience* **9**(1), 77–82 (2016).

Self, S., T.Thordarson, M. Widdowson, Gas Fluxes from Flood Basalt Eruptions, *Elements* **1** (5), 283–287 (2005). doi: https://doi.org/10.2113/gselements.1.5.283.

Self, S., M. Widdowson, T. Thordarson, A.E. Jay, Volatile fluxes during flood basalt eruptions and potential effects on the global environment: A Deccan perspective, *Earth and Planetary Science Letters* **248**(1-2), 518-532 (2006).

Sherwood, S.C., M. Huber, An adaptability limit to climate change due to heat stress, *Proceedings of the National Academy of Sciences* **107** (21), 9552-9555 (2010). doi:10.1073/pnas.0913352107
Sobolev, S., Sobolev, A., Kuzmin, D. *et al.*, Linking mantle plumes, large igneous provinces and environmental catastrophes, *Nature* **477**, 312–316 (2011). https://doi.org/10.1038/nature10385

Solomon, S.C., M.A. Bullock, D.H. Grinspoon, Climate Change as a Regulator of Tectonics on Venus, *Science* **286**, 5437, 87-90 (1999). DOI: 10.1126/science.286.5437.87

Song, H., D.B. Kemp, L. Tian, L. *et al.*, Thresholds of temperature change for mass extinctions, *Nat Commun* **12**, 4694 (2021). doi:10.1038/s41467-021-25019-2

Sosdian, S.M., T.L. Babila, R. Greenop, *et al.,* Ocean Carbon Storage across the middle Miocene: a new interpretation for the Monterey Event, *Nat Commun* **11**, 134 (2020). https://doi.org/10.1038/s41467-019-13792-0

Stoffel, M., M. Khodri, C. Corona *et al.,* Estimates of volcanic-induced cooling in the Northern Hemisphere over the past 1,500 years, *Nature Geosci* **8**, 784–788 (2015). https://doi.org/10.1038/ngeo2526

Strahan, S.E., B.N. Duncan, P. Hoor, Observationally derived transport diagnostics for the lowermost stratosphere and their application to the GMI chemistry and transport model, *Atmos. Chem. Phys.* **7**, 2435–2445 (2007). doi: 10.5194/acp-7-2435-2007

Tong, J.A., Y. You, R.D. Müller, M. Seton, Climate model sensitivity to atmospheric CO_2 concentrations for the middle Miocene, *Global Planet. Change* **67**, 129–140 (2009).

Vellekoop, J., A.Sluijs, J. Smit, S. Schouten, J. W. H.Weijers, J. S. Sinninghe Damsté, H. Brinkhuis, Rapid short-term cooling at K–Pg boundary, *Proceedings of the National Academy of Sciences* **111** (21), 7537-7541 (2014). DOI:10.1073/pnas.1319253111

Way, M.J., A.D. Del Genio, I. Aleinov et al., Climates of Warm Earth-like Planets I. 3D Model SImulations, The Astrophysical Journal Supplemental Series **239**, 24 (2018). doi: 10.3847/1538-4365/aae9e1

Wignall, P.B., Large igneous provinces and mass extinctions, *Earth Sci. Rev.* **53**, 1–33 (2001).

Wolf, E.T., OB. Toon, The evolution of habitable climates under the brightening Sun. *J. Geophys. Res. Atmos.* **120**, 5775– 5794 (2015). doi: 10.1002/2015JD023302.

You, Y., M. Huber, R.D. Müller, C.J. Poulsen, J. Ribbe, Simulation of the Middle Miocene Climate Optimum, *Geophys. Res. Lett.* **36**, L04702 (2009). doi:10.1029/2008GL036571

Zambri, B., A.N. LeGrande, A. Robock, J. Slawinska, Northern Hemisphere winter warming and summer monsoon reduction after volcanic eruptions over the last millennium, *J. Geophys. Res. Atmos.* **122**, 7971– 7989 (2017). doi:10.1002/2017JD026728

344

345